Electron Spin Polarization of Functionalized Fullerenes. Reversed Quartet Mechanism

Vladimir Rozenshtein,[†] Alexander Berg,[†] Eli Stavitski,[†] Haim Levanon,*[,†,‡] Lorenzo Franco,[§] and Carlo Corvaja*[,§,⊥]

Department of Physical Chemistry and The Farkas Center for Light-Induced Processes, The Hebrew University of Jerusalem, Jerusalem 91904, Israel, and Department of Chemical Sciences, University of Padova, via Marzolo 1, 35131, Padova, Italy

Received: July 20, 2005; In Final Form: October 10, 2005

Time-resolved electron paramagnetic resonance (TREPR) spectroscopy was used to study two functionalized fullerenes consisting of a C_{60} moiety covalently linked to TEMPO radical via spacers of different length. Photoinduced electron spin polarization (ESP) reflecting a non-Boltzmann population within the energy levels of the spin system was observed in the electronic ground and excited states. Both fullerenes are characterized by a sign inversion of their TREPR spectra. A new mechanism of ESP generation was suggested to explain the experimental results. This mechanism, termed as the reversed quartet mechanism (RQM), includes the intersystem crossing process, which generates ESP in the excited trip-doublet and trip-quartet ($^2T_1$ and $^4T_1$) states. This ISC is accompanied by ESP transfer to the ground state ($^2S_0$) by either electron-transfer reaction (in our case via charge transfer state, ^{2}CT, i.e., $^2T_1 \rightarrow {}^2\text{CT} \rightarrow {}^2S_0$) or internal conversion, $^2T_1 \rightarrow {}^2S_0$.

Introduction

It was reported recently on the photoexcited rigidly bound radical−triplet systems, where electron spin polarization (ESP) was found to invert its sign in a microsecond time scale.[1−4] Such temporal behavior is characterized by the EPR spectra, initially in emission turning into absorption or vice versa.[1−3] Signal inversion was found both in covalently linked C_{60}−nitroxide radical systems[1−3] and in porphyrin−nitroxide radical ligated complexes.[4] In contrast to the case of radical−triplet encounter pairs in liquids, where only ESP of the ground-state radicals is detected,[5−8] in the case of rigid systems, ESP of the excited states are also observed.[1−4]

We report here on a mechanistic study of ESP generated in covalently linked radical−triplet pairs (RTPs), where mutual translational motion is absent. Under such conditions, the conventional radical−triplet pair mechanism (RTPM) is not operative.[5−8] Therefore, a new polarization mechanism, based on the effects of spin selective interactions within the photoexcited molecule, is presented.

This work is an extension of recent studies of copper porphyrins[8b] and chromium metallocorrole,[8c] characterized by large spin exchange interaction (of several hundreds of wavenumbers), and of functionalized fullerenes[1,2] with small spin exchange interaction (of a few wavenumbers), where the tetrapyrroles or C_{60} moieties were photoexcited to their triplet states, allowing radical−triplet interactions to generate ESP. Two closely related fullerenes (**1** and **2**, Scheme 1), consisting of C_{60} covalently linked to TEMPO radical (C_{60}−TEMPO) via different spacers, were investigated. In both compounds, the C_{60}−TEMPO separation distances are comparable to the diameter of C_{60}. Both systems, when photoexcited, are characterized by a sign inversion of the time-resolved EPR (TREPR) spectra. To understand the mechanism, by which this phenomenon occurs, we have carried out a series of experiments over a wide range of temperatures, covering liquid and solid states of the solvents, with the C_{60}−TEMPO concentrations, spanning over 2 orders of magnitude.

SCHEME 1

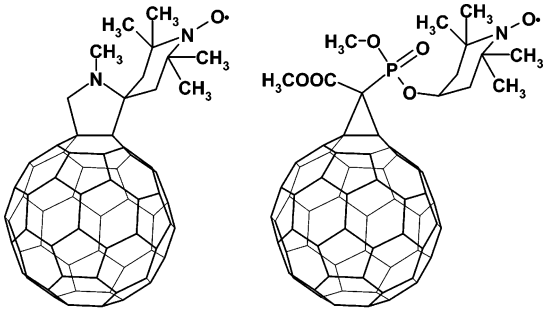

1 **2**

Experimental Section

1 and **2** (*N*-methyl fulleropyrrolidine−TEMPO and methanofullerene−TEMPO), consisting of C_{60} and the TEMPO radical (2,2,6,6 tetramethylpiperidine-1-oxyl) covalently linked via a pyrrolidine ring or a methanephosphate group, respectively, were synthesized as described elsewhere.[9,10] EPR samples were prepared in 4 mm o.d. Pyrex tubes, degassed by several freeze−pump−thaw cycles on a vacuum line and sealed under vacuum. The concentration of **1** and **2** in toluene and *o*-dichlorobenzene (DCB) was 10^{-4} to 5×10^{-3} M. Steady-state EPR and TREPR measurements were carried out with Bruker ESP 380 spectrometer interfaced to OPO (Continuum Panther II-10; 2−3 mJ/pulse, 10 Hz repetition rate, ∼10 ns pulse duration) pumped by the third harmonic (355 nm) of the Nd:YAG laser (Surelite II-10), Varian E-line EPR spectrometer interfaced to the Nd:YAG laser (Continuum 661-20, 2−4 mJ/pulse, 20 Hz repetition rate, ∼10 ns pulse duration) and Bruker ER 200D EPR spectrometer

* Corresponding author.
† The Hebrew University of Jerusalem.
‡ E-mail: levanon@chem.ch.huji.ac.il.
§ University of Padova.
⊥ E-mail: carlo.corvaja@unipd.it.

10.1021/jp0540104 CCC: $30.25
Published on Web 11/19/2005

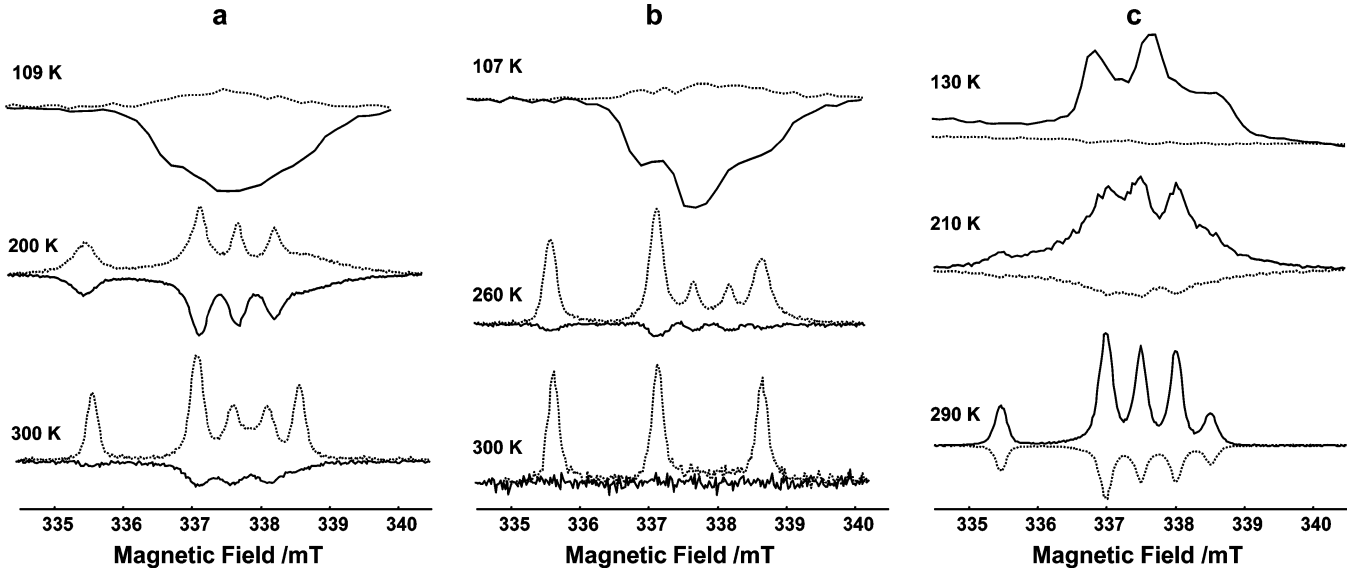

Figure 1. Photoinduced TREPR spectra of **1** and **2**. Spectra shown for each temperature refer to the maximal emissive and absorptive signals. Solid lines: initial spectra recorded at 0.3 μs after the laser pulse; dotted lines: spectra recorded at 1.5 μs after the laser pulse. Key: (a) **1** in toluene; (b) **1** in *o*-dichlorobenzene; (c) **2** in toluene.

interfaced to the Nd:YAG laser (Continuum 661-20 or Quantel Brilliant; 2−4 mJ/pulse, 20 Hz repetition rate, ∼10 ns pulse duration). The TREPR signals were taken directly from the preamplifier and transferred to the digital oscilloscope (LeCroy 9400 or LeCroy LT 342) after being passed through a broadband amplifier (20 dB). EPR signals were acquired on a PC through a GPIB interface. The spectra were reconstructed from the full set of data over a chosen magnetic field range. The response times of the TREPR setups were 150−200 ns. The temperature was controlled (with accuracy of 1 K) by a variable-temperature nitrogen-flow Dewar located inside the EPR cavity.

Samples were excited by the 532 nm radiation. The magnetic field was calibrated using the EPR signal of 1,1-diphenyl-2-picrylhydrazyl ($g = 2.0036$). In all systems studied, the kinetic traces were independent of the microwave power in the range between 20 and 200 mW, implying that the kinetics reflect spin dynamics without effects associated with saturation phenomena.[11]

Results

Figure 1 exhibits typical photoinduced TREPR spectra of **1** in toluene (a) and DCB (b) and **2** in toluene (c), at different temperatures. These spectra were taken at two time windows, corresponding to the maximum emission and the maximum absorption (Figure 2). At $T \leq 315$ K, for **1** in toluene (a) and DCB (b), all spectra start in emission, evolving into absorption. At $T \leq 290$ K, for **2** in toluene (c), the initial absorptive spectra evolve into emissive spectra at later times.

For both **1** and **2**, the initial extremum is observed at about 200−500 ns after the laser pulse, while the following extremum appears several microseconds later. The characteristic temperatures, where the spectral changes occur, strongly depend on the solvent and, likely, relate to the liquid−glass transition temperatures. It is noteworthy that the time, which corresponds to the ESP sign change, does not depend on the concentrations, while the EPR signal intensity is concentration dependent.

Three temperature regions were considered for each solvent: (1) $T > T_H$ (high temperatures, liquid), (2) $T < T_L$ (low temperatures, solid), and (3) $T_L < T < T_H$ (intermediate temperatures, soft glass). T_H and T_L are ∼210 and 140 K for toluene and ∼260 and 250 K for DCB, respectively.

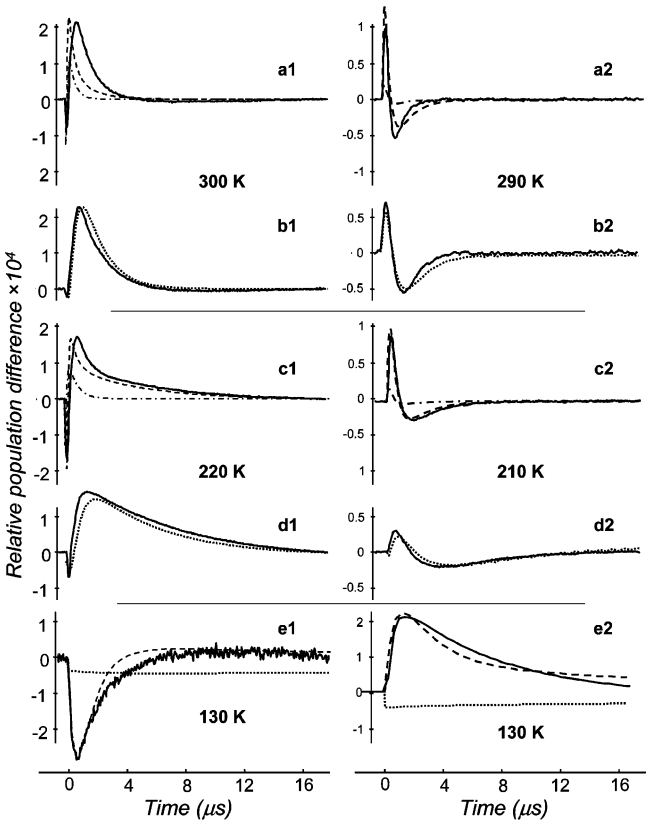

Figure 2. Experimental kinetic traces (arbitrary units) vs simulated temporal dependences of relative population differences for compound **1** (left column, a1−e1) and for compound **2** (right column, a2−e2). Solid lines: experimental traces of the excited (a1, c1, e1 and a2, c2, e2) and ground (b1, d1 and b2, d2) states. Dashed lines: simulated curves describing the overall population difference of the excited states ($^2T_1 + {}^4T_1$; see text for details). Dash−dotted lines: calculated traces of the population differences of the trip-doublet state ($^2T_1$). Dotted lines: calculated traces of the population differences of the ground state ($^2S_0$).

In the high-temperature region, the five-line TREPR spectra are observed for both **1** and **2**.[1] Figure 3, part 1, shows the spectrum of **1** taken in DCB at 650 ns after the laser pulse. Figure 3, part 2, depicts the spectrum of **2** taken in toluene at

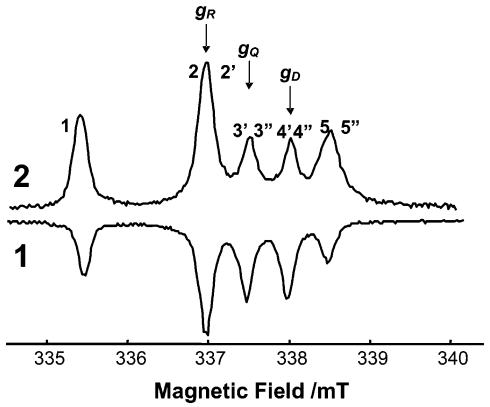

Figure 3. (1) TREPR spectrum of photoexcited **1** (DCB, 260 K, 650 ns after laser pulse); (2) TREPR spectrum of photoexcited **2** (toluene, 290 K, 1500 ns after laser pulse).

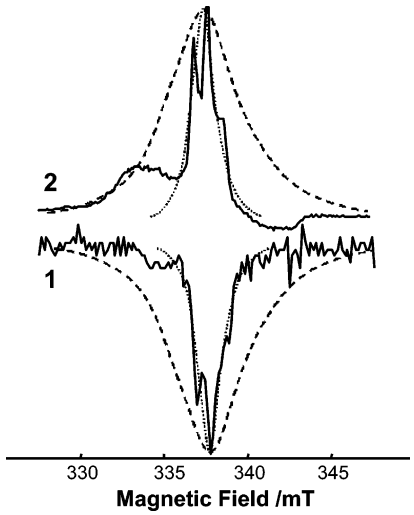

Figure 4. Solid lines: experimental TREPR spectra of **1** and **2** in glassy toluene matrix (120 and 115 K, respectively). Dashed lines: integrated (and inverted in case **1**) steady-state EPR spectrum of **1** and **2**. Dotted lines: the same as dashed but 3-fold narrowed.

1500 ns after the laser pulse. The field positions of the EPR lines do not depend on the temperature and the solvent. Typical kinetic traces, obtained at $T > T_H$ (300 K for **1** and 290 K for **2**) in toluene, taken at field positions 1 and 3′/3″ (Figure 3, part 1), are presented in Figure 2 (parts a1, b1 and parts a2, b2).

At low temperature ($T < T_L$), the observed spectra are poorly resolved. Figure 4 depicts very early spectra obtained at 120 and 115 K for **1** and **2**, respectively. The spectrum of **1** exhibits three strongly overlapped lines, while that of **2** also includes three intense overlapping lines in the middle but with two additional broad outermost lines (absorptive peak at low magnetic field and emissive peak at high field). For **1**, identical spectra and kinetics were observed in both solvents. The corresponding kinetic traces are shown in Figure 2 (parts e1 and e2).

In the intermediate region, $T_L < T < T_H$, spectra represent a mixture of the spectra for high and low temperatures (Figure 1). Such intermediate regime exists in toluene solutions and practically is absent in DCB.

Discussion

The EPR Spectra. To a good approximation, each of **1** and **2** can be considered as consisting of two separate entities, i.e., C_{60} and TEMPO, located at a fixed distance from each other. The center-to-center distance was estimated to be 8 Å for **1** and 11 Å for **2**.[12] For **1** and **2** compounds, the distance between the radical NO and the "surface" of C_{60} was found to be 4 and 7 Å, while the distance between the radical NO and the "equator" of C_{60} was estimated to be 7 and 10 Å.[12] Chemical bonding, via the pyrrolidine or phosphate bridges, does not involve electrons responsible for the stable spin ($S = {}^1/_2$), localized on TEMPO, and for the photoinduced spin ($S = 1$), localized on the equator of C_{60}.[13] These three valence electrons are involved in the formation of the lower electronic excited states of **1** and **2**. In such systems, the exchange interaction between two electrons of C_{60} moiety is much larger than the exchange interaction of these electrons with the uncoupled electron of TEMPO moiety. Thus, the full Hamiltonian can be replaced by an effective one, which operates only on the radical and triplet spin variables (S_R and S_T, respectively). In other words, the line positions of the EPR spectra of the excited states of **1** and **2** can be found by taking into account only the exchange and magnetic interactions within the intramolecular doublet−triplet pairs. With such an approach, the two electrons of C_{60} moiety are coupled by the "doublet−doublet" spin exchange, $H_{ex}^{DD} = -2J_{DD}S_aS_b$, while the three electrons of the doublet and triplet moieties are coupled by the "doublet−triplet" spin exchange interaction, $H_{ex}^{DT} = -2J_{DT}S_RS_T$, where J_{DD} and J_{DT} are the exchange integrals; $S_T = S_a + S_b$; and S_a, S_b are the spin operators of each of the two triplet C_{60} electrons, a and b, respectively. The major contributions to J_{DT} are the direct spin exchange and the superexchange through the bridge. The latter includes the spin superexchange itself and the exchange via intramolecular electron transfer (ET), to generate the charge transfer state, $^2CT \equiv {}^2(^2C_{60}^-; {}^1TEMPO^+)$. Because of the relatively large distance between the triplet and doublet components, the direct exchange, operating due to overlapping of orbitals of C_{60} and TEMPO, is negligible.[14] On the other hand, the superexchange, induced by the delocalization of electrons on the pyrrolidine or phosphate bridge may be of a few cm^{-1}.[15,16] Detection of the EPR spectra of "pure" excited doublet and quartet states supports the above estimate. In such a case, where J_{DT} is larger than the magnetic interactions within the system (strong exchange limit),[17] the exchange interaction removes the spin degeneracy forming the excited doublet and quartet states separated by ΔE_{DT} ($= 3J_{DT}$). In the opposite case of the weak exchange limit, where J_{DT} is smaller than the magnetic interactions, the excited doublet and quartet states are no longer pure spin states and the EPR spectra should show separate resonances close to the *g*-values of the individual centers (C_{60} and TEMPO, in our case).[17] Such spectra must depend on both J_{DT} and D_{TR} (the dipole−dipole interaction between S_R and S_T) and are split into multiplets when J_{DT} value is smaller than the *g*-value difference between centers.[17] In our case, $J_{DT} > 0$ for **1** and $J_{DT} < 0$ for **2**, implying that the quartet state lies below the excited doublet state and vice versa, respectively.[1] Eigenfunctions of the systems can be approximately described by the product of the eigenfunctions of the C_{60} and TEMPO parts.[17] The first excited eigenstates of **1** and **2** can be referred to as a "sing-doublet" ($^2S_1$), "trip-doublet" ($^2T_1$) and "trip-quartet" ($^4T_1$) with "sing" and "trip" indicating either a singlet or triplet configuration of the π-electrons of C_{60} and pointing out on a dual character of the system.[18] For **1**, these states are schematically shown in the energy diagram of Figure 5a. For **2**, a similar diagram is valid except that the $^2T_1$ state lies below the $^4T_1$ state (not shown). Energies of the $^2T_1$

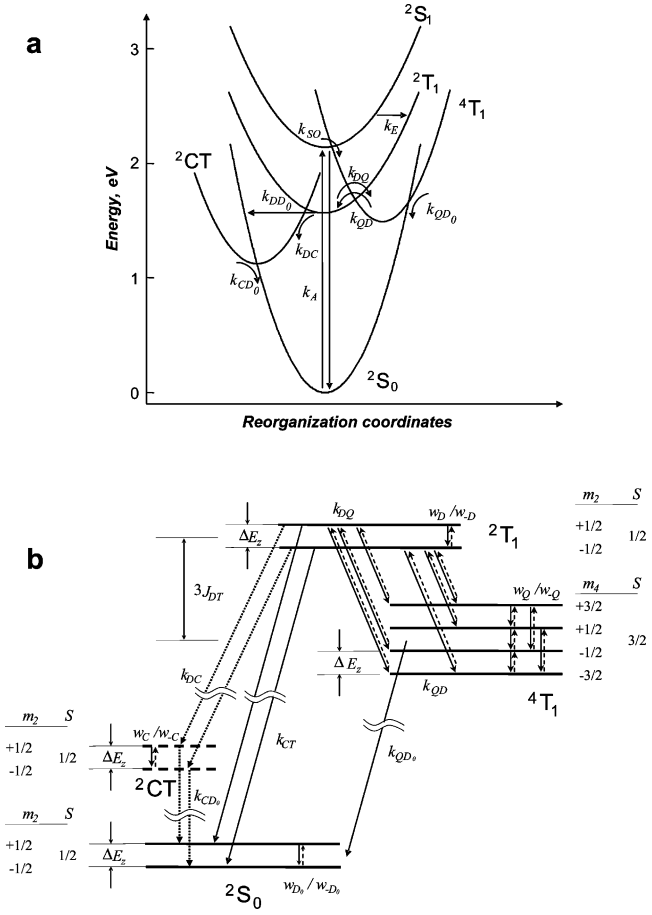

Figure 5. (a) Energy diagram of C_{60}−TEMPO ensembles. (b) Kinetic scheme of processes involved in ESP generation.

and $^4T_1$ states are close to that of the $^3T_1$ state of C_{60}, which is located at $\Delta E_{D-D} = 2J_{DD} \approx 0.2$ eV below the $^2S_1$ state (cf. Figure 5a).

In the strong exchange limit the $^2T_1$ and $^4T_1$ states are described phenomenologically by separate spin Hamiltonians. Thus, the *g*-factor and hyperfine splitting (hfs) parameters of the $^2T_1$ (g_D and A_D) and $^4T_1$ (g_Q and A_Q) states can be expressed by the linear combinations of the corresponding values of C_{60} and TEMPO:[17]

$$g_D = -\frac{1}{3}g_R + \frac{4}{3}g_T \quad (1)$$

$$A_N^D = -\frac{1}{3}A_R^N \quad (2)$$

$$g_Q = \frac{1}{3}g_R + \frac{2}{3}g_T \quad (3)$$

$$A_Q^N = \frac{1}{3}A_R^N \quad (4)$$

where g_R and g_T are the *g*-factors of TEMPO and $^{3*}C_{60}$, respectively, and A_R^N is the hfs parameter of TEMPO. In the control experiments, we measured separately the isotropic EPR parameters of TEMPO and $^{3*}C_{60}$ ($g_R = 2.0060$, $g_T = 2.0014$, and $A_R = 15.35$ G), which are in a good agreement with those obtained previously.[1,19,20] With these data and eqs 1−4 we calculate $g_D = 1.9998$, $g_Q = 2.0029$, $A_D = -5.1$ G, and $A_Q = 5.1$ G. These calculated parameters can be compared with the experimental ones extracted from the field positions of the EPR lines (cf. Figure 3). Such comparison shows that the field positions of lines labeled 1, 2, and 5 are in agreement with those calculated for the ground state spectrum of TEMPO while the field positions of lines labeled 2′, 3′, 4′ and 3″, 4″, 5″ correspond to the $^2T_1$ and $^4T_1$ states, respectively. We conclude that the five lines of the TREPR spectra of **1** and **2**, observed in the liquid phase, can be considered as a superposition of three triplets of lines corresponding to the following: (1) the ground state ($^2S_0$) of **1** or **2** with a line separation of 15 G; (2) two excited states ($^2T_1$ and $^4T_1$) with a line separation of 5 G in each spectrum. Both the ground state and excited state spectra consist of the three equidistant lines due to hfs.

Upon temperature decrease, the TREPR spectra undergo significant changes, when a well-resolved pattern turns into broad, almost-unresolved lines (Figures 1). It should be emphasized that even for liquid solutions the ground state spectrum of TEMPO, in equilibrium, is not fully isotropic, namely, (1) the different hf lines are of different intensity, and (2) the line shapes are not Lorentzian. It is due to fact that even fast molecular motion cannot average the large anisotropy of the *g*- and hf interaction tensors. In glassy environment, the dipolar interaction within the clusters formed in frozen solutions broadens the TREPR spectra as well.[21] The intermediate temperature region between T_H and T_L correlates with that between T_M and T_G, where T_M is the melting point (178 K for toluene and 256 K for DCB) and T_G is the glass transition temperature (117.5 K for toluene and 170 K for DCB).[22,23]

Contrary to the liquid phase, in the glassy environment, the hfs constants and the *g*-factors cannot be rigorously determined because of line broadening. Nevertheless, analysis of the spectral shape of the broadened lines allows identifying the observed species. The analysis is based on the fact that, in the slow motion regime, the hf lines overlap and, thus, the width of the EPR spectrum is dictated by the hfs constant. In Figure 4 (dashed lines), we show the integrated steady-state EPR spectra of **1** and **2**, attributed to the TEMPO moiety. Such spectrum of **1** is inverted in addition. These spectra are presented together with the photoinduced TREPR spectra of **1** and **2** (solid lines). Also shown are the computer-simulated spectra (dotted lines), obtained upon compression by a factor of 3 the scale of the magnetic field for the dashed-line spectra. According to eqs 2 and 4, this narrowed spectrum simulates the spectrum of the $^2T_1$ or $^4T_1$ state. In particular, the line width of the low-temperature spectrum is close to that of the simulated spectrum (Figure 4). It implies that, in glassy samples, we observe excited states only. Unfortunately, we cannot distinguish between the $^2T_1$ and $^4T_1$ states because of a relatively small difference between their *g* values ($\Delta g = 0.0029$). Thus, both states correspond to the broad central peak of the spectra taken at low temperature. If these spectra include a contribution of the quartet state then, in principle, the two outermost anisotropic lines of $^4T_1$ could be observed together with the central line.[24,25] The spectra shown in Figure 4 are displayed on an expanded scale, as compared to the spectra shown in Figure 1. It is demonstrated that we are dealing with a single line (structured by hfs) for **1** and with three anisotropic lines for **2 (**the central line is also structured by hfs**)**. The central line of **2** represents the sum of several contributions, namely the following: (1) the Zeeman transition within the $^2T_1$ manifold; (2) the $-1/2 \leftrightarrow +1/2$ transition within the $^4T_1$ manifold, which involves contributions from all orientations of the quartet with respect to the magnetic field, and (3) minor contributions from the tails of the outermost lines corresponding to the $\pm 3/2 \leftrightarrow \pm 1/2$ transitions. The single structured line of **1** also includes the contribution from the $-1/2 \leftrightarrow +1/2$ transitions within both $^4T_1$ and $^2T_1$ manifolds, while

the $\pm^3/_2 \leftrightarrow \pm^1/_2$ transitions are not observed. The outermost lines originate from transitions corresponding mainly to the perpendicular orientation of the rotational molecular axis with respect to the magnetic field.[24,25] Such outermost lines should be separated from the central line by the distance equal to $D_Q/g_e\beta_B$, where D_Q is the ZFS parameter of the quartet state.[24] A rough estimate of D_Q can be obtained, using the expression $D_Q = (^1/_3)D_T + (^1/_3)D_{TR,}$[17] where D_T is the ZFS parameter of the triplet moiety ($D_T/g_e\beta_B \approx -100$ G for C_{60})[26] and D_{TR} relates to the dipolar interaction between the triplet and radical constituents. Thus, neglecting the contribution of the second term, which is expected to be small due to the relatively large intramolecular triplet−radical distance, we obtain the fact that the central and outermost anisotropic lines have to be separated approximately by 30−40 G. This figure is in line with observed separation between outermost anisotropic lines (75 G) of the quartet state of **2**. It is also close to that obtained for the compound similar to those used in this study.[27] Since $D_Q < 0$, the low-field outermost spectral wing is attributed to the $-^1/_2 \leftrightarrow -^3/_2$ transition and the high-field one relates to the $+^1/_2 \leftrightarrow +^3/_2$ transition.[24] While for **2** we have detected all three anisotropic lines, for **1** the outer lines escape EPR detection (Figure 4). This apparent discrepancy will be discussed below.

Mechanism of Spin Polarization.

1. General Remarks. To elucidate an ESP mechanism, several experimental observations should be taken into account: (1) in the liquid and soft glass, we observe simultaneously the TREPR spectra of the ground doublet, excited trip-doublet and trip-quartet states; (2) in the solid glass, only the excited states are detected; (3) the early spectra of **1** start in an emission mode, evolving into an absorption mode and vice versa for **2**; (4) the characteristic times of the ESP generation do not depend on the concentration of C_{60}−TEMPO.

We consider the ESP mechanism by taking into account the intramolecular magnetic interactions between the radical (R) and the photoexcited triplet ($^3T_1$) within C_{60}-TEMPO. The energy states, which participate in the ESP formation, are shown in Figure 5a. The intramolecular charge transfer (CT) state associated with the ET reaction between two parts of the molecule (^{2}CT) is also presented. The CT interactions are often considered as the dominant interactions for triplet quenching of aromatic molecules (including fullerenes) by nitroxyl radicals.[28−31] The energy of ^{2}CT is equal to that required for ET from TEMPO to C_{60}:[32,33]

$$E_{CT} = eE_{ox}(\text{TEMPO}) - eE_{red}(C_{60}) - e^2/\epsilon r_s \qquad (5)$$

where $E_{red} = -(0.46 \div 0.54)$ V[34,35] and $E_{ox} = +(0.55 \div 0.87)$ V,[31,34] are the reduction potential of C_{60} and the oxidation potential of TEMPO vs SCE, respectively; e is the electron charge, ϵ is the dielectric constant, and r_s is the distance between donor and acceptor (spacer length). Neglecting the Coulombic interaction of the charged products, one obtains $E_{CT} = 1.0$−1.4 eV, which is the upper-limit value. Thus, ^{2}CT lies below $^2T_1/^4T_1$, allowing the latter to be quenched via CT reactions.[36]

2. Reversed Quartet Mechanism. RTPM cannot explain the present results. It is due to the fact that our systems possess rigid covalent structures with fixed triplet−radical distances. In such a case, there is no mutual diffusive motion of the interacting paramagnetic species as required.[5−8,37] For intermolecular cases, the ESP generation via RTPM could be principally expected during encounters between the triplet part of one C_{60}−TEMPO molecule and the radical part of the other C_{60}−TEMPO molecule. However, such a route can be also neglected, since we observed that ESP is generated in time scale of 200 ns, independent of the C_{60}−TEMPO concentration. This figure is in contradiction with the estimated time of 10 μs (for the diffusion-limited process at low concentrations of 10^{-4} M). Moreover, the RTPM cannot account for the ESP sign reversal. In addition, at any particular time the ESP sign of the ground and excited states was found to be the same (cf. Figure 1). This observation also contradicts RTPM, which is a spin sorting process only, i.e., it neither creates nor destroys magnetization. In such a case, signs of the radical and triplet ESP should be opposite. Because ESP of the quartet state of fullerenes has to follow that of the triplet state of C_{60} moiety, the ESP sign of the quartet must differ from that of the radical.

ESP transfer (ESPT) mechanism cannot account for the observed ESP as well.[37,38] In the framework of ESPT, polarization of the triplet part is generated due to a fast selective ISC and then it is "transferred" to the TEMPO part. For the intermolecular case, ESPT is not operative by the same reasons outlined above for RTPM, while for intramolecular case, two mechanisms of ESPT, namely the energy transfer mechanism[39] and the direct spin exchanged mechanism,[40] should be considered. The former mechanism cannot occur since the first excited state of TEMPO lies higher than the triplet state of the C_{60} part.[41] The latter mechanism is discarded since the ESP of both triplet fullerene derivatives is absorptive, whereas we detected an initial emission for **1** and absorption for **2**.

In view of the above consideration, we propose a new mechanism, which can account for the initial emissive polarization and the subsequent absorptive polarization or vice versa. This mechanism, termed as reversed quartet mechanism (RQM), includes ISC, which generates ESP within the excited $^2T_1$ and $^4T_1$ states. Such ISC is accompanied by the ESP transfer to the ground state, $^2S_0$ (by either the ET reaction or the $^2T_1 \rightarrow {}^2S_0$ internal conversion (IC)). These processes are schematically depicted in Figure 5a. The term RQM stems from its formal similarity with reversed triplet mechanism applied earlier to the triplet radical ion pairs,[42,43] where triplet sublevels are depleted selectively to the singlet ground state, and concurrently, the triplet forms radical products in the course of the chemical reaction. In such a case, the products can manifest a net ESP when ISC competes with the chemical reaction and the spin relaxation within the triplet manifold. In the following sections, we will discuss the processes participating in RQM.

(i) Processes Occurring During the Laser Pulse. During the laser pulse, several processes manage to be completed, namely photoexcitation (k_A), sing-doublet → trip-doublet IC (k_E) and sing-doublet → trip-quartet ISC (k_{SO}).

The excited doublet state $^2S_1$ is formed due to photoexcitation of the C_{60} moiety. The extinction coefficients of **1** and **2** at 532 nm were found to be of 1200 M^{-1} cm^{-1}, which is close to that of the pristine C_{60}. Thus, the effective rate constant of light absorption, k_A ($=\sigma I$) is 2×10^6 s^{-1},[44] where σ ($= 2 \times 10^{-18}$ cm^2) is the absorption cross section of C_{60}−TEMPO and I ($\approx 10^{24}$ photons/cm^2) is the photon flux per unit area. For simplicity, we make a reasonable assumption, confirmed by the simulations, that the characteristic time of the overall quenching responsible for the ESP generation is longer than duration of the laser pulse ($\tau_p = 10^{-8}$ s). As a result, we obtain that only ~2% of the molecules are excited. All other molecules (98%) remain in the ground state,$^2S_0$, during the entire photoinduced cycle. In such a case, light absorption itself results in the simultaneous depletion (2%) of both ground-state Zeeman sublevels. It implies that ESP is reduced by 3.3×10^{-5} (at 130 K) with respect to equilibrium value, and thus, such ESP manifests itself as the initial "emissive" TREPR signal (after

subtraction of the equilibrium signal). In our systems, the above-described "optical" ESP is several times weaker then ESP generated via RQM.

During the laser pulse, two processes populate $^2T_1$: the indirect process via fast spin−orbit induced ISC within the C_{60} moiety, $^1S_1 \rightarrow {}^3T_1$ (5×10^8 s^{-1}),[45] and the direct process via the $^2S_1 \rightarrow {}^2T_1$ IC, while the $^4T_1$ state can be populated only via the ISC.

As a result of indirect process (ISC and the radical−triplet interaction), the photoexcited $^2S_1$ state is converted rapidly to the spin polarized $^2T_1$ and $^4T_1$ states. Since the difference in the Zeeman energies of the doublet (TEMPO) and triplet (^{3}*C_{60}) spins is much less than J_{DT}, the eigenfunctions of the spin Hamiltonian describe pure doublet and quartet spin states. For the doublet state they can be expressed as follows:[17]

$$\left|{}^2T, +\frac{1}{2}\right\rangle = \frac{1}{\sqrt{3}}(-|T_0\rangle|\alpha\rangle + \sqrt{2}|T_{+1}\rangle|\beta\rangle)$$

$$\left|{}^2T, -\frac{1}{2}\right\rangle = \frac{1}{\sqrt{3}}(-|T_0\rangle|\beta\rangle + \sqrt{2}|T_{-1}\rangle|\alpha\rangle) \quad (6)$$

where $|T_0\rangle$ and $|T_{+1}\rangle$ are the near-high-field eigenfunctions of the ^{3}*C_{60} substates and $|\alpha\rangle$ and $|\beta\rangle$ are those of the up and down Zeeman states of the TEMPO moiety, respectively.

The analogous eigenfunctions of trip-quartet substates are[17]

$$\left|{}^4T, +\frac{3}{2}\right\rangle = |T_{+1}\rangle|\alpha\rangle$$

$$\left|{}^4T, +\frac{1}{2}\right\rangle = \frac{1}{\sqrt{3}}(\sqrt{2}|T_0\rangle|\alpha\rangle + |T_{+1}\rangle|\beta\rangle)$$

$$\left|{}^4T, -\frac{1}{2}\right\rangle = \frac{1}{\sqrt{3}}(\sqrt{2}|T_0\rangle|\beta\rangle + |T_{-1}\rangle|\alpha\rangle)$$

$$\left|{}^4T, -\frac{3}{2}\right\rangle = |T_{-1}\rangle|\beta\rangle \quad (7)$$

Since the ZFS parameter of ^{3}*C_{60} is relatively small, the triplet wave functions can be considered in the high-field approximation. In such a case, we may neglect the magnetic selectivity and, based on eqs 6 and 7, claim that initially all six Zeeman sublevels will be equally populated with no contribution to the initial polarization.

Direct transition from $^2S_1$ is the second route to populate $^2T_1$. Such transition is partially allowed due to mixing of $^2S_1$ and $^2T_1$ induced by the nonequivalent exchange in three-electron system, namely by the interaction of two electrons of the C_{60} triplet moiety with one electron of the TEMPO doublet moiety.[18,46] Furthermore, the matrix element $|\langle {}^2S_1|H_{ex}^{DT}|{}^2T_1\rangle|$ was shown to be proportional to the Coulomb integral Q_C.[46] Since Q_C does not depend on spin variables, the exchange-induced transitions are not spin selective.

(ii) Trip-Doublet ↔ Trip-Quartet ISC (k_{DQ} and k_{DQ}). The radiationless transition rate constant, k_{DQ}, between the Zeeman sublevels of $^2T_1$ and $^4T_1$ (labeled as $m_2 = \pm 1/2$ and $m_4 = \pm 1/2$, $\pm 3/2$, respectively), can be expressed as the product of the zero point motion rate constant, k_{DQ}^{00} ($=10^{13}-10^{14}$ s^{-1}), the Franck−Condon factor, FC, and the prohibition factor due to change of the spin, f_S (m_2,m_4): [47]

$$k_{DQ}(m_2,m_4) = k_{DQ}^{00} \times FC \times f_s(m_2,m_4) = k_{DQ}^{0} \times f_s(m_2,m_4) \quad (8)$$

Since the energy gap between $^2T_1$ and $^4T_1$ is small (i.e., $3J_{DT}$ is much smaller than the vibrational quanta) and the vibrational relaxation within the $^2T_1$ state is very fast, the transition occurs between the zeroth vibrational levels of $^2T_1$ and $^4T_1$. In such a case, two important consequences can be derived. First, one should expect a large overlap between the initial and final vibrational eigenfunctions and, as a result, FC should be large. Second, the doublet-quartet ISC becomes reversible, in contrast to the case of a large energy gap, where a fast vibrational relaxation within the final state makes the back ISC practically forbidden. Since in our case $3J_{DT} \gg \Delta E_Z$ (where ΔE_Z is the energy gap between two neighboring Zeeman sublevels), the ratio $k_{QD}(m_4, m_2)/k_{DQ}(m_2,m_4) = \exp(-3J_{DT}/kT) \approx 0.98$ is valid for any of the allowed doublet−quartet transitions. The backward quartet−doublet ISC will be shown below to be responsible for the inversion of the ESP sign found in **1** and **2**. From perturbation theory, we can obtain the values of f_s:

$$f_s(m_2,m_4) = |\langle {}^4T_1(m_4)|H_{ZFS}|{}^2T_1(m_2)\rangle|^2/\Delta E(m_2,m_4)^2 \quad (9)$$

where $\Delta E(m_2,m_4) = E[^2T_1(m_2)] - E[^4T_1(m_4)]$. Transitions, allowed due to the ZFS interaction, are listed in Table 1, together with the corresponding matrix elements, averaged over the angles of the magnetic field direction in the dipolar interaction tensor principal axes.[1] Taking into account the energy gaps between various pairs of the Zeeman sublevels, we obtain the magnitudes of $k_{DQ}(m_2,m_4)$ (Table 1). The appropriate magnitudes of the parameters involved are also shown in Table 1. In Figure 6, we show the respective population distributions over the Zeeman sublevels of $^4T_1$, neglecting the quenching and spin lattice relaxation (SLR) processes. Such distributions relate only to very early times after photoexcitation. They show an excess of population in the highest and lowest energy levels of the quartet state.

TABLE 1. Parameters of Trip−Doublet ↔ Trip−Quartet Intersystem Crossing

transition[a]	transition matrix element[b]	energy gap[c] 1	energy gap[c] 2	transition rate[d] 1	transition rate[d] 2
$+1/2 \rightarrow +3/2$	$1/45 D_T^2$	$3J - \Delta E_z$	$-3J + \Delta E_z$	1.4	0.20
$-1/2 \rightarrow +3/2$	$1/45 D_T^2$	$3J - 2\Delta E_z$	$-3J + 2\Delta E_z$	1.1	0.19
$-1/2 \rightarrow +1/2$	$1/135 D_T^2$	$3J - \Delta E_z$	$-3J + \Delta E_z$	0.5	0.07
$+1/2 \rightarrow -1/2$	$1/135 D_T^2$	$3J + \Delta E_z$	$-3J - \Delta E_z$	0.4	0.08
$+1/2 \rightarrow -1/2$	$1/45 D_T^2$	$3J + 2\Delta E_z$	$-3J - 2\Delta E_z$	1.0	0.24
$-1/2 \rightarrow -1/2$	$1/45 D_T^2$	$3J + \Delta E_z$	$-3J - \Delta E_z$	1.1	0.22

[a] $^2T_1(m_2) \rightarrow {}^4T_1(m_4)$. [b] $\langle {}^4T_1(m_4)|\boldsymbol{H}_{ZFS}|{}^2T_1(m_2)\rangle^2_{av}$. [c] $^{\Delta}E(m_2,m_4)$. [d] $k_{DQ}^0 \times \{\langle {}^4T_1(m_4)|\boldsymbol{H}_{ZFS}|{}^2T_1(m_2)\rangle_{av}^2/\Delta E(m_2,m_4)^2\} \times 10^{-6}$ s^{-1}. $k_{DQ}^0 = 1.5 \times 10^{13}$ s^{-1}, $J = 1.7$ cm^{-1}, $|D_T| = 10^{-2}$ cm^{-1} for **1**. $k_{DQ}^0 = 10^{13}$ s^{-1}, $J = -3.4$ cm^{-1}, $|D_T| = 10^{-2}$ cm^{-1} for **2**.

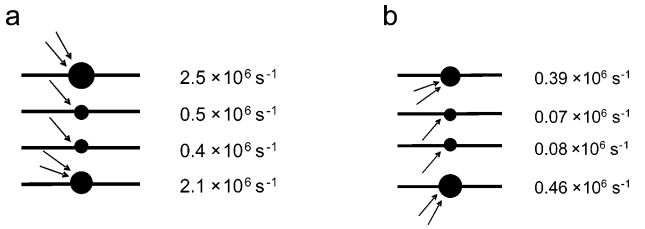

Figure 6. Population distributions over the Zeeman sublevels of the $^4T_1$ state at early times after photoexcitation, obtained for **1** (a, $J_{DT} > 0$) and **2** (b, $J_{DT} < 0$) by using the transition rates shown in Table 1.

(iii) Polarization Transfer to Ground State (k_{DD_0} and k_{DC}/k_{CD_0}). Polarization transfer to the ground state will be discussed in terms of Figure 5a. Two routes can account for such a transfer

with the conservation of the spin projection. The first is $^2T_1 \rightarrow {}^2S_0$ (IC, k_{DD_0}) and the second route is the successive forward and backward ET, i.e., $^2T_1 \rightarrow {}^2CT \rightarrow {}^2S_0$ (k_{DC} and k_{CD_0}, respectively). It is known that the nonadiabaticity operator is responsible for both the IC and ET transitions between the adiabatic electronic states.[48,49] This operator does not act explicitly on the spin variables and, as a result, both IC and ET transitions between states of equal multiplicity do not change the spin alignment. However, in our systems, the ET route is apparently more efficient because of several reasons. First, CT formation is considered as the major pathway for triplet quenching of aromatic molecules by nitroxyl radicals.[28,29] Second, ET and back ET (BET) may occur with a considerable activation energy (as was actually found for our systems), while IC is expected to be activationless. Activationless character is anticipated since IC occurs via tunneling (as a result of a small mutual displacement of the $^2T_1$ and $^2S_0$ potentials along the reorganization coordinate). Third, the $^2T_1 \rightarrow {}^2S_0$ IC is accompanied by the $^3T_1 \rightarrow {}^1S_0$ ISC, a process which depends on the spin and, thus, does not conserve the spin alignment. As a result, we will not consider the IC route as compatible with the CT route. As to the CT route itself, we cannot determine which one of the two successive ET processes (forward ET or backward ET) is the rate-limiting stage. Simulations of the kinetic traces show that the ESP dynamics does not depend on a specific choice. Therefore, utilizing the generalized effective rate constant, $k_{CT} = (k_{DC}{}^{-1} + k_{CD_0}{}^{-1})^{-1}$ and assuming, for a definiteness, that ET is slower than BET, we get $k_{CT} \approx k_{DC}$. In such a case, taking into account that the electron is transferred from the TEMPO part to the C_{60} part over the distance r_{CT}, the rate constant can be expressed as follows:[50,51]

$$k_{CT} = k_{CT}{}^{00} \times \exp(-E_A/kT) = k_{CT}{}^{0} \times \exp[-\beta r_{CT}] \exp(-E_A/kT) \quad (10)$$

where $k_{CT}{}^0 = 2\pi\alpha_0{}^2/\{\hbar(4\pi\lambda kT)^{1/2}\}$ is the preexponential factor, α_0 is the contact electronic coupling matrix element (for intramolecular ET, $\alpha_0 \approx 200-400$ cm^{-1}), λ is the reorganization energy ($\approx$1000 cm^{-1}), β is a constant of about 1−2 Å^{-1}, $E_A = \{-(\Delta G + \lambda)^2/4\lambda\}$ is the activation energy of the ET reaction, and ΔG is the free energy of reaction. On the basis of the above values, we obtain $k_{CT}{}^0 \approx 10^{14}$ s^{-1}, and thus, $k_{CT}{}^0 \times \exp[-\beta r_{CT}] \approx 10^{10}$ s^{-1} for $r_{CT} \approx 8$ Å, i.e., for the distance typical for the C_{60}−TEMPO compounds under study.[12] Indeed, the simulations, carried out for **1** and **2**, indicate that for $T = 107-315$ K the polarization transfer to the ground state is an activated process (see below). It implies that the ET reactions are involved in the quenching process with the rate constant expressed by eq 10. The simulations provide us with $E_A = (3.5 \pm 0.3)$ and (2.3 ± 0.3) kcal/mol and $k_{CT}{}^{00} = 7.0 \times 10^9$ and 2.2×10^8 s^{-1} for **1** and **2**, respectively. With $k_{CT}{}^0$ and β taken as 10^{14} s^{-1} and 1.2 Å^{-1}, we obtain that $r_{CT} = 8$ and 11 Å for **1** and **2**, respectively. These figures are in line with the separation distances between the C_{60} and TEMPO moieties obtained by molecular modeling.

(iv) Spin−Lattice Relaxation (w_D/w_{-D}, w_Q/w_{-Q}, and w_{D_0}/w_{-D_0}). To simulate the ESP dynamics, one should take into account the SLR processes. We took into account both the forward and backward transitions with the respective rate constants w_S and w_{-S}, ($S = D$, D_0, and Q for $^2T_1$, $^2S_1$, and $^4T_1$, respectively). We utilized the single-quantum SLR transitions between the magnetic sublevels, taking into account the principle of detailed balancing, i.e., that $w_{-S} = w_S \exp(-\Delta E_z/kT)$.[52,53] Since SLR within the quartet state is induced by fluctuations of the ZFS interaction, which considerably exceeds the magnetic interactions in the doublet states, we expect that $w_{D_0} \approx w_D < w_Q$.

(v) Kinetic Scheme. The reversed quartet mechanism can be discussed in terms of Figure 5b, which depicts the processes related to the ESP generation. Light absorption (k_A) acting during 10 ns and the prompt populating of the $^2T_1$ and $^4T_1$ levels (k_E and k_{SO}, respectively), are considered as the initial conditions. More specifically, based on the above discussion, we assume that at very short time, which we consider as the zero time, the relative populations of the Zeeman sublevels of $^2S_0$, $^2T_1$ and $^4T_1$ are as follows: $[^2S_0(-^1/_2)]_0 = 0.98[^2S_0(-^1/_2)]_{eq}$; $[^2S_0(+^1/_2)]_0 = 0.98[^2S_0(+^1/_2)]_{eq}$; $\lambda[^4T_1(-^3/_2)]_0 = \lambda[^4T_1(-^1/_2)]_0 = \lambda[^4T_1(+^1/_2)]_0 = \lambda[^4T_1(+^3/_2)]_0 = [^2T_1(-^1/_2)]_0 = [^2T_1(+^1/_2)]_0$, where subindex "eq" stands for the equilibrium populations and λ is the parameter indicating the initial population distributions between the $^2T_1$ and $^4T_1$ states. From simulations, we have $\lambda = 2$ and 3 for **1** and **2**, respectively.

EPR detects a component of the magnetization, perpendicular to the external magnetic field ($M_\perp$), while a component, parallel to this field ($M_{||}$), is associated with the population difference Δn between the Zeeman sublevels involved in the microwave induced transition. Generally, temporal behavior of the magnetization is described by the modified Bloch equations, which together with the spin−lattice and phase relaxation terms, characterized by the respective relaxation times $T_1 = w_S{}^{-1}$ and T_2, include also terms accounting for the electronic quenching and chemical processes.[54] In our case, TREPR signal is changed with a characteristic time longer than T_2. Thus, the derivative of the perpendicular magnetization components with respect to time can be safely taken as zero. As a result, $M_\perp$ (and corresponding EPR signal) is proportional to the product $T_2 \times \omega_1 \times \Delta n$, where $\omega_1 = (g\beta_B/\hbar)B_1$, g is the g-factor of the transition and B_1 is the amplitude of the microwave field.[55] In addition, since we do not observe microwave saturation effects, we can neglect the microwave field term in the equation for Δn. The above considerations imply that, in our case, analysis of the EPR signals can be replaced by analysis of the respective populations.

The populations of the Zeeman sublevels of the ground and excited states were found by numerical solutions of the set of coupled balance equations with the rate constants described in previous sections:

$$d\boldsymbol{P}/dt = \boldsymbol{W}\boldsymbol{P} \quad (11)$$

where $\boldsymbol{P}$ is the column vector with components, which represent the populations of the individual sublevels, and $\boldsymbol{W}$ is the matrix with elements comprised of the linear combinations of the rate constants of the processes involved. Equation 11 is presented in expanded form in Appendix I.

The simulations should take into account the concurrent behavior of three paramagnetic species, reflected as kinetics of different overlapping lines of the same EPR spectrum. Thus, in this procedure, we need to calculate the absolute populations of the Zeeman sublevels of the different electronic states and to assign them to the intensities of all observed lines. To satisfy the above requirements, instead of the true population differences we introduce and utilize the effective population differences, namely, that of the excited states, Δn(ES), that of the ground state, Δn(GS), and that of the trip-doublet state, Δn(D). The definitions of these quantities are presented in Appendix II.

Simulations were carried out for different temperatures. To fit in the effective population differences with the EPR signal

amplitudes, the input parameters J_{DT}, k_{DQ}^0, λ, E_A, w_{D_0}, w_D, w_Q, and k_{QD_0} were varied. Results of the simulations are displayed in Figure 2, superimposed on the relevant experimental data. These traces are presented by taking into account several instrumental effects, described in Appendix II.

Results of Simulation. The results, obtained within the framework of RQM, explain the dynamic behavior of ESP, characterized by the sign inversion of the EPR signal. RQM describes the behavior of both the excited and ground states and explains the temperature and environment dependences of ESP.[57,58] We have verified that together with the $^4T_1$ state, the $^2T_1$ state contributes considerably to the observed overall ESP of the excited states (cf. Figure 2). As to the $^2T_1 \rightarrow {}^4T_1$ ISC, the best simulations were obtained with $k_{DQ}^0 = 1.5 \times 10^{13}$ s^{-1} at high temperatures and $(0.3 \div 0.5) \times 10^{13}$ s^{-1} at low temperatures, for both **1** and **2**.

The simulations also provide us with the SLR rates within the $^4T_1$, $^2T_1$, and $^2S_0$ manifolds. In liquid solutions, w_Q is of $(2 \div 3) \times 10^7$ s^{-1} for **1**, while for **2** w_Q was found to be slower ($\approx 10^6$ s^{-1}). These values are comparable to k_{CT}. In the glassy solutions, w_Q is slower than in liquid solutions, namely of $(2 \div 3) \times 10^5$ s^{-1} for both **1** and **2**. It turns out that the calculated kinetic curves, particularly the time when ESP changes its sign, are sensitive to values of w_Q. This is the case because SLR within the trip-quartet state strongly affects, via the $^2T_1 \leftrightarrow {}^4T_1$ and $^2T_1 \rightarrow {}^2S_0$ processes, the population of $^2T_1$ and $^2S_0$ states. On the other hand, the time dependences were found to be insensitive to variations of w_D ($(1-5) \times 10^5$ s^{-1}). For **1** and **2**, the magnitude of the SLR rate of the ground state, w_{D_0}, was found to change from 10^4 s^{-1} (100 K) to 3×10^5 s^{-1} (300 K).

Data on the SLR rates within multiplet states (triplet, quartet, etc.) in liquids are scarce.[59,60] For the triplet state of pristine C_{60}, SLR was found to occur with the rate of 3×10^6 s^{-1} in toluene at room temperature.[61] This figure is the intermediate between those obtained in the present study for the quartet states of **1** and **2**. Apparently, SLR within the quartet and triplet states is governed by fluctuations of the ZFS interaction with a rate dictated by the values of the ZFS parameters and the fluctuation correlation time τ_C.[52] Since ZFS values of **1** and **2** are close, the difference between their SLR rates is determined, most likely, by different τ_C values associated with different molecular size and shape. The low-temperature value of w_Q obtained here is also close to the triplet SLR rates.[62] Summarizing this part, we conclude that SLR of the quartet and triplet states apparently results from similar mechanisms.

With the data obtained by the simulations, we can analyze the populations of the Zeeman sublevels and the related EPR signal amplitudes over a wide range of temperatures. Results obtained for low temperature are shown in Figure 2 (parts e1, e2). For both **1** and **2**, the light-induced population differences of the ground state were found to be negligibly small as compared to those of the excited states. This is in line with experiments where only EPR transitions within the $^2T_1$ and $^4T_1$ states were observed, while the ground-state molecules escape detection. The reason is that the ET rate was shown to decrease considerably by lowering the temperature. Thus, the ESP transfer to the ground-state becomes slower than SLR within the excited states and, as a result, ESP relaxes to its equilibrium value prior to repopulating the ground state. For the excited states of **2**, the $-1/2 \leftrightarrow +1/2$ transition of $^2T_1$ and all three anisotropic transitions of $^4T_1$ ($-1/2 \leftrightarrow +1/2$, $-1/2 \leftrightarrow -3/2$ and $+1/2 \leftrightarrow +3/2$) were detected, while for **1**, the two outermost lines attributed to the $-1/2 \leftrightarrow -3/2$ and $+1/2 \leftrightarrow +3/2$ transitions were not observed.[24,25] The reason for that is as follows. The ratio between the amplitudes of the outer and central resonances (κ_P) can be presented as a product of the analogous ratio for the equilibrium spectrum (κ_P^E) and the ratio of the corresponding nonequilibrium population differences ($\kappa_{NE} = |\Delta n(\pm 3/2, \pm 1/2)/\Delta n(-1/2, +1/2)| \equiv |([^4T_1(\pm 3/2)] - [^4T_1(\pm 1/2)])/([^4T_1(-1/2)] - [^4T_1(+1/2)])|$), i.e., $\kappa_P = \kappa_P^E \times \kappa_{NE}$. A powder EPR spectrum of the equilibrium quartet state was analyzed previously.[24] In this study, the intensity distribution between the peaks was found to depend strongly on D_Q and the transition broadenings, W_0 for the $-1/2 \leftrightarrow +1/2$ transition and W_1 for the $\pm 1/2 \leftrightarrow \pm 3/2$ transitions. Using expressions derived in ref 24 and assuming that $W_0 = W_1$, for $D_Q/g_e\beta_B = 40$ G and the transition broadening of 5 G, we obtain $\kappa_P^E = 0.01$. The value of D_Q was estimated above, and the value of W_0 was obtained from the line width of the hf component of the central peak (W_1 cannot be found because of an absence of outermost peaks for **1** and full overlapping of the hf components of the outermost lines for **2**). On the other hand, the simulations show that the population differences $\Delta n(-3/2, -1/2)$ and $\Delta n(+3/2, +1/2)$ considerably exceed $\Delta n(-1/2, +1/2)$, i.e., κ_{NE} may be as much as 10 (Table 1). Nevertheless, even for the above κ_{NE} value, κ_P is close to 0.1. As a result, the outer resonances escape detection since the *S*/*N* ratio was found to be of 10 (cf. the low-temperature spectra of **1**, Figure 4). Thus, the intensity of the outermost lines is estimated to be on the verge of the experimental sensitivity. Apparently, minor variations of D_Q, W_0, and W_1 may allow one to detect these lines for **2** (cf. Figure 4) and escape their detection for **1**.[63] The genesis of the absorption/emissive pattern of the outermost lines of **2** (Figure 4) can be illustrated by the population scheme shown in Figure 6. Obviously, since "the outermost sublevels" ($m_4 = +3/2$ and $-3/2$) are overpopulated compared to "the inner sublevels" ($m_4 = +1/2$ and $-1/2$), the $-1/2 \leftrightarrow -3/2$ and $+1/2 \leftrightarrow +3/2$ transitions should be detected in the absorption and emission modes, respectively.

We found that the ISC rate constant of $^4T_1 \rightarrow {}^2S_0$ is practically same for the both compounds ($k_{QD_0} = (3-5) \times 10^4$ s^{-1}), independent of the temperature and the state of solutions. It is worth noting that these values are in line with the quartet lifetimes ($25-50$ μs) reported elsewhere.[19,64] At low temperatures (cf. Figure 2, parts e1 and e2) this ISC contributes to the decay of ESP. At higher temperatures, the activated CT process turns to be much faster than the ISC quenching, and thus, the latter can be neglected.

Regarding the exchange interaction, the best-fit values of J_{DT} were found to be $+1.7$ and -3.4 cm^{-1}, for **1** and **2** respectively. These values are comparable with those estimated previously for a compound similar to those studied here.[65] With these findings, the energy gaps $3J_{DT}$ between the $^2T_1$ and $^4T_1$ states are sufficiently large so that a difference in the rates of the forward and back ISC ($^2T_1 \leftrightarrow {}^4T_1$) could govern the kinetic behavior of the system, ensuring a change of ESP sign. Changing the sign of J_{DT} from positive to negative results in changing the order of ESP: the emission/absorption sequence switches to the absorption/emission one.

An important point to discuss is the relationship between the sign of J_{DT} and the value of r_{CT}. The separation distances between the nitroxide radical and fullerene moieties are large, with the shorter distance (8 Å) related to $J_{DT} > 0$ (**1**) and the longer distance (11 Å) related to $J_{DT} < 0$ (**2**). For such relatively large distances, direct overlap of the electronic clouds is negligibly small. Thus, the indirect interactions, induced by delocalization of the electrons over the bridge connecting the doublet and triplet moieties (spin superexchange) and/or by ET

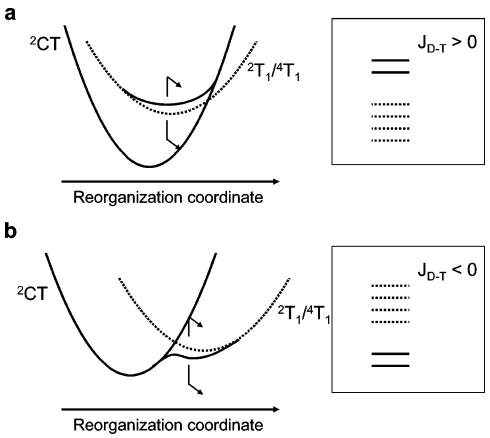

Figure 7. Intersections between the doublet-quartet ($^2T_1/^4T_1$) and charge-separated (^{2}CT) states. Electronic potentials of the states involved are shown as the sections of energy surfaces through the reorganization coordinate. Solid and dotted lines belong to states of doublet and quartet multiplicity, respectively. The insets show the sections of energy surfaces for the coordinate corresponding to the distance between the doublet and the triplet constituents (enlarged scale). Two cases are shown: intersections in the inverted (a) and the normal (b) regions.

between those moieties, could account for the spin exchange. We assume that ET interactions are dominant suggesting a qualitative model based on mixing between $^{2,4}T_1$ and ^{2}CT states. In Figure 7, we present the parabolic electronic potentials of the doublet-quartet $\{^{2,4}T_1 \equiv {}^{2,4}(^3C_{60};\ ^2\text{TEMPO})\}$ and charge-separated $\{^2\text{CT} \equiv {}^2(^2C_{60}{}^-;\ ^1\text{TEMPO}^+)\}$ states. They are the cross sections of the energy surfaces through the inner-sphere reorganization coordinate. The solid and dotted lines belong to the doublet and quartet multiplicities, respectively. The unperturbed $^2T_1$ and $^4T_1$ states are shown as degenerate since the direct overlapping between states is negligibly small for large separations. The insets to Figure 7 show the potentials, which correspond to the separation distance between the constituents of the radical−triplet pair, subjected to the external magnetic field. We assume that in the intersection region the wave function of the doublet charge separated state, ^{2}CT, is mixed with that of the $^2T_1$ state, implying that the transferred electron is shared by both interacting moieties. Two cases are considered: (a) intersections in the inverted region and (b) intersections in the normal region. When the degenerate $^{2,4}T_1$ potential crosses the ^{2}CT potential in the inverted region, the former is selectively destabilized, namely the ^{2}CT and $^2T_1$ states with the same multiplicity are mixed in the crossing region, while $^4T_1$ remains intact (cf. Figure 7a). Destabilization of the $^2T_1$ state as compared to the $^4T_1$ state is associated with removal of the $^{2,4}T_1$ degeneracy resulting in $J_{DT} > 0$. On the other hand, in the normal region, stabilization of the $^2T_1$ state occurs (cf. Figure 7b), and thus, the gap between the $^2T_1$ and $^4T_1$ states is described by $J_{DT} < 0$. On the basis of the ESP observations we conclude that crossing of the potentials occurs in the inverted region for **1** (resulting in $J_{DT} > 0$) and in the normal region for **2** (resulting in $J_{DT} < 0$). From this model, the normal region is related to the larger C_{60}−TEMPO distance (**2**), while the shorter distance (**1**) is associated with the inverted region. Supporting evidence for the above conclusion can be found in recent analytical approaches, which took into account effect of the CT states on the exchange interaction between two doublet species.[16,66,67] In these studies, it was shown that for large distances between spins, J_{DD} can be approximated by $\{-V_{RP}{}^2/(\Delta G_{ET} + \lambda_{ET})\}$, where V_{RP} is the matrix element coupling the reactant and product electronic states, ΔG_{ET} and λ_{ET} are the free and reorganization energies of a particular ET reaction. Thus, for cases where $(-\Delta G_{ET}) > \lambda_{ET}$, i.e., in the Marcus inverted region, $J_{DD} > 0$ while for $(-\Delta G_{ET}) > \lambda_{ET}$, i.e., in the Marcus normal region, $J_{DD} < 0$.

Conclusions

On the basis of the experimental observations of ESP, generated in liquid and frozen solutions of two C_{60}−TEMPO compounds, a new mechanism, RQM, operating in rigid systems, was proposed. With this mechanism, we could explain all qualitative features of the observed ESP under different experimental conditions. As a result of the simulations in the framework of RQM, we succeeded in getting the rates of the relaxation processes occurring between and within the lower electronic states of the functionalized fullerenes.

Acknowledgment. We thank Prof. M. Maggini of the Department of Chemical Sciences of the University of Padova and Prof. I. A. Nuretdinov of The Arbuzov Institute of Organic and Physical Chemistry of Kazan for providing samples of fullerenes, Dr. M. Mazzoni of the Department of Chemical Sciences of the University of Padova for help in running experiments. This work was supported by Italian MIUR (Contract No. 2002032171 and FIRB Contract No. RBNE01P4JF) (C.C. and L.F.). The work at The Hebrew University of Jerusalem was supported by the Humboldt Foundation, Israel Science Foundation, the U.S.−Israel Binational Science Foundation (H.L.), and the KAMEA Foundation (V.R. and A.B.). We are thankful to R. Rubin for editing the text and figures.

Appendix I

The populations of the Zeeman sublevels are given by the solving the coupled kinetic equations:

$$\frac{d[^2T_1(+^1/_2)]}{dt} = -\{k_{DQ}(+^1/_2,+^3/_2) + k_{DQ}(+^1/_2,-^1/_2) + k_{DQ}(+^1/_2,-^1/_2) + w_D + k_{DD_0}(+^1/_2,+^1/_2)\}[^2T_1(+^1/_2)] + k_{QD}(+^3/_2,+^1/_2)[^4T_1(+^3/_2)] + k_{QD}(-^1/_2,+^1/_2)[^4T_1(-^1/_2)] + k_{QD}(-^3/_2,+^1/_2)[^4T_1(-^3/_2)] + w_{-D}[^2T_1(-^1/_2)]$$

$$\frac{d[^2T_1(-^1/_2)]}{dt} = -\{k_{DQ}(-^1/_2,+^3/_2) + k_{DQ}(-^1/_2,+^1/_2) + k_{DQ}(-^1/_2,-^3/_2) + w_{-D} + k_{DD_0}(-^1/_2,-^1/_2)\}[^2T_1(-^1/_2)] + k_{QD}(+^3/_2,-^1/_2)[^4T_1(+^3/_2)] + k_{QD}(+^1/_2,-^1/_2)[^4T_1(+^1/_2)] + k_{QD}(-^3/_2,-^1/_2)[^4T_1(-^3/_2)] + w_D[^2T_1(+^1/_2)]$$

$$\frac{d[^4T_1(+^3/_2)]}{dt} = -\{k_{QD}(+^3/_2,-^1/_2) + k_{QD}(+^3/_2,-^1/_2) + w_Q(+^3/_2,+^1/_2) + w_Q(+^3/_2,-^1/_2) + k_{QD_0}\}[^4T_1(+^3/_2)] + k_{DQ}(+^1/_2,+^3/_2)[^2T_1(+^1/_2)] + k_{DQ}(-^1/_2,+^3/_2)[^2T_1(-^1/_2)] + w_{-Q}(+^1/_2,+^3/_2)[^4T_1(+^1/_2)] + w_{-Q}(-^1/_2,+^3/_2)[^4T_1(-^1/_2)]$$

$$\frac{d[^4T_1(+^1/_2)]}{dt} = -\{k_{QD}(+^1/_2,-^1/_2) + w_{-Q}(+^1/_2,+^3/_2) + w_Q(+^1/_2,-^1/_2) + w_Q(+^1/_2,-^3/_2) + k_{QD_0}\}[^4T_1(+^1/_2)] + k_{DQ}(-^1/_2,+^1/_2)[^2T_1(-^1/_2)] + w_Q(+^3/_2,+^1/_2)[^4T_1(+^3/_2)] + w_{-Q}(-^1/_2,+^1/_2)[^4T_1(-^1/_2)] + w_{-Q}(-^3/_2,+^1/_2)[^4T_1(-^3/_2)]$$

$$\frac{d[^4T_1(-^1/_2)]}{dt} = -\{k_{QD}(-^1/_2,+^1/_2) + w_{-Q}(-^1/_2,+^3/_2) + w_{-Q}(-^1/_2,+^1/_2) + w_Q(-^1/_2,-^3/_2) + k_{QD_0}\}[^4T_1(-^1/_2)] + k_{DQ}(+^1/_2,-^1/_2)[^2T_1(+^1/_2)] + w_Q(+^3/_2,-^1/_2)[^4T_1(+^3/_2)] + w_Q(+^1/_2,-^1/_2)[^4T_1(+^1/_2)] + w_{-Q}(-^3/_2,-^1/_2)[^4T_1(-^3/_2)]$$

$$\frac{d[^4T_1(-^3/_2)]}{dt} = -\{k_{QD}(-^3/_2,-^1/_2) + k_{QD}(-^3/_2,-^1/_2) + w_{-Q}(-^3/_2,+^1/_2) + w_{-Q}(-^3/_2,-^1/_2) + k_{QD_0}\}[^4T_1(-^3/_2)] + k_{DQ}(+^1/_2,-^3/_2)[^2T_1(+^1/_2)] + k_{DQ}(-^1/_2,-^3/_2)[^2T_1(-^1/_2)] + w_Q(+^1/_2,-^3/_2)[^4T_1(+^1/_2)] + w_Q(-^1/_2,-^3/_2)[^4T_1(-^1/_2)]$$

$$\frac{d[^2S_0(+^1/_2)]}{dt} = k_{DD_0}(+^1/_2,+^1/_2)[^2T_1(+^1/_2)] - w_{D_0}[^2S_0(+^1/_2)] + w_{-D_0}[^2S_0(-^1/_2)] + \frac{k_{QD_0}}{2}\{[^4T_1(+^3/_2)] + [^4T_1(+^1/_2)] + [^4T_1(-^1/_2)] + [^4T_1(-^3/_2)]\}$$

$$\frac{d[^2S_0(-^1/_2)]}{dt} = k_{DD_0}(-^1/_2,-^1/_2)[^2T_1(-^1/_2)] + w_{D_0}[^2S_0(+^1/_2)] - w_{-D_0}[^2S_0(-^1/_2)] + \frac{k_{QD_0}}{2}\{[^4T_1(+^3/_2)] + [^4T_1(+^1/_2)] + [^4T_1(-^1/_2)] + [^4T_1(-^3/_2)]\}$$

Appendix II

To compare the calculated populations with the experimental TREPR signals obtained in liquid solutions, in terms of the amplitude of the specific lines, several important points should be taken into account.

(1) The lines of the excited states (2/2″, 3′/3″, 4′/4″, and 5/5″ in Figure 3) represent a superposition of several EPR signals occurring due to different Zeeman transitions. For liquid samples, they include transitions within both $^2T_1$ and $^4T_1$ states (which are undistinguishable for X-band EPR due to accidental coincidence of the magnetic fields corresponding to the *g*-factors difference and the hfs parameters of these excited states). Contribution of $^4T_1$ therewith contains all anisotropic transitions of the $^4T_1$ state merging into a single line by molecular motion.[24]

(2) Since the width of the lines are comparable with the distances between them, the broad non-Lorentzian tails of the ground state lines affect the amplitude of lines ascribed to the excited states. This effect is strongly temperature dependent.

3) We should take into account that every component, contributing to the line intensity, is proportional to $\Delta n g^2 \beta_B^2 S(S+1)(B_0/\Delta B_{1/2})$,[55] where B_0 is the magnetic field strength corresponding to the center of the component, and $\Delta B_{1/2}$ is the half-width of the component (fwhm). In other words, one should take into account different spin values, *g*-values, and width of every line component.

On the basis of the above arguments, for comparing the calculated values with the experimental TREPR signals, we utilize the effective population differences instead of the real population differences. In Figure 2, we plot the following quantity for the population difference of the excited states:

$$\Delta n(ES) = \alpha_1\{0.75([^4T_1(-^3/_2)] - [^2T_1(-^1/_2)]) + ([4T_1(-^1/_2)] - [^2T_1(+^1/_2)]) + 0.75([^4T_1(-^3/_2)] - [^2T_1(-^1/_2)])\} + ([^2T_1(-^1/_2)] - [^2T_1(+^1/_2)]) + \alpha_2\alpha_3([^2S_0(-^1/_2)] - [^2S_0(+^1/_2)]) \quad \text{(AII-1)}$$

and for that of the ground state:

$$\Delta n(GS) = \alpha_3\{([^2S_0(-^1/_2)] - [^2S_0(+^1/_2)]) - ([^2S_0(-^1/_2)]_{eq} - [^2S_0(+^1/_2)]_{eq})\} \quad \text{(AII-2)}$$

where $\alpha_1 = \{^3/_2(^3/_2+1)\}/\{^1/_2(^1/_2+1)\} = 5$ and $\alpha_2 = 0.1-0.3$, depending on temperature (a contribution of the ground-state line wing). α_3 (=0.8) accounts for the line width difference; $([^2S_0(-^1/_2)]_{eq} - [^2S_0(+^1/_2)]_{eq}) = \Delta n_{eq}(GS)$ is the equilibrium population difference. For illustration, we also show in Figure 2 the temporal dependence of the virtual signal of $^2T_1$ state, which experimentally cannot be sorted out:

$$\Delta n(D) = ([^2T_1(-^1/_2)] - [^2T_1(+^1/_2)]) \quad \text{(AII-3)}$$

To compare simulated and experimental results, we should take into account a few instrumental effects. First, although we observe negative EPR signals both for the excited and ground states (Figure 2), they correspond to the emissive ESP for the $^2T_1$ and $^4T_1$ states only, but not for the ground state. A reason for that is associated with a specificity of TREPR technique. The preamplifier of the TREPR spectrometer includes a filter, which cuts the low-frequency components of the incoming signal together with a constant equilibrium signal. To take this effect into account, we have subtracted an equilibrium population difference from the calculated values (cf. eq AII-2).[56] For both **1** and **2** at all temperatures used, $|\Delta n(GS)|$ was found to be smaller than $\Delta n_{eq}(GS)$. It means that, although the "apparent" EPR signals of the ground states look like being emissive, actually we have a strong deviation from equilibrium, associated with absorption of microwaves. In contrast, for the excited states we observed real emissive spectra because of the zero equilibrium populations. The second instrumental effect is connected with the fact that the initial ESP evolves within the response time of EPR spectrometer and, thus, the corresponding EPR spectra appear less intense then the "true" ones. To match the theoretical and experimental results we convoluted the computed temporal functions with the Gauss response function of the spectrometer (100 ns fwhm).

References and Notes

(1) Corvaja, C.; Maggini, M.; Ruzzi, M.; Scorrano, G.; Taffoletti, A. *Appl. Magn. Reson.* **1997**, *12*, 477.
(2) Sartori, E.; Toffoletti, A.; Corvaja, C.; Garlaschelli, L. *J. Phys. Chem. A* **2001**, *105*, 10776.
(3) Mazzoni, M.; Conti, F.; Corvaja, C. *Appl. Magn. Reson.* **2000**, *18*, 351.
(4) Fujisawa, J.; Ishii, K.; Ohba, Y.; Yamauchi, S.; Fuhs, M.; Möbius, K. *J. Phys. Chem. A* **1999**, *103*, 213.
(5) Blättler, C.; Jent, F.; Paul, H. *Chem. Phys. Lett.* **1990**, *166*, 375.
(6) Kawai, A.; Obi, K. *Res. Chem. Intermed.* **1993**, *19*, 865.
(7) Shushin, A. I. *Chem. Phys. Lett.* **1999**, *313*, 246.
(8) (a) Rozenshtein, V.; Zilber, G.; Rabinovitz, M.; Levanon, H. *J. Am. Chem. Soc.* **1993**, *115*, 5193. (b) Rozenshtein, V.; Berg, A.; Levanon, H.; Krueger, U.; Stehlik, D.; Kandrashkin, Yu., van der Est, A. *Isr. J. Chem.* **2003**, *43*, 373. (c) Stavitski, E.; Berg, A.; Ganguly, T.; Mahammed; Gross, Z.; Levanon, H. *J. Am. Chem. Soc.* **2004**, *126*, 6886.

(9) Arena, F.; Bullo, F.; Conti, F.; Corvaja, C.; Maggini, M.; Prato, M.; Scorrano, G. *J. Am. Chem. Soc.* **1997**, *119*, 789.

(10) Gubskaya, P.; Berezhnaya, L. S.; Yanilkin, V. V.; Morozov, V. I.; Nastarova, N. V.; Efremof, Y. Y.; Nuretdinov, I. A. *Russ. Chem. Bull.* **2005**, in press.

(11) Furrer, R.; Fujara, F.; Lange, C.; Stehlik, D.; Vieth, H. M.; Vollmann, W. *Chem. Phys. Lett.* **1980**, *75*, 332.

(12) This distance between the N atom and the C_{60} was calculated by HyperChem software.

(13) Visser, J.; Groenen, E. J. J. *Chem. Phys. Lett.* **2002**, *356*, 43.

(14) Molin, Y. N.; Salikhov, K. M.; Zamaraev, K. I. *Spin Exchange, Principles and Applications in Chemistry and Biology*; Springer: New York, 1980.

(15) Teki, Y.; Miyamoto, S.; Nakatsuji, M.; Miura, Y. *J. Am. Chem. Soc.* **2001**, *123*, 294.

(16) Calvo, R.; Abresch, E. C.; Bittl, R.; Feher, G.; Hofbauer, W.; Isaacson, R. A.; Lubitz, W.; Okamura, M. Y.; Paddock, M. L. *J. Am. Chem. Soc.* **2000**, *122*, 7327.

(17) Bencini, A.; Gatteschi, D. *EPR of Exchange Coupled Systems*; Springer: Berlin, 1990.

(18) Gouterman, M. In *The Pophyrins*; Dolphin, D., Ed.; Academic Press: New York, 1978; Vol. 3; p 1.

(19) Steren, C. A.; Levstein, P. R.; Van Willigen, H.; Linschitz, H.; Biczok, L. *Chem. Phys. Lett.* **1993**, *204*, 23.

(20) Levanon, H.; Meiklyar, V.; Michaeli, A.; Michaeli, S.; Regev, A. *J. Phys. Chem.* **1992**, *96*, 6128.

(21) Space distribution of guest molecules in disordered media affects observed EPR spectra. In glasses, the guest molecules are dispersed inhomogeneously to form clusters, where the distances between the particles are much smaller than the calculated average distance for the relevant concentration of the solute.[68] TEMPO molecules in ethanol and water-glycerol glasses form clusters with the average intermolecular distances of 25 Å, while distance, averaged over all the sample, is 60 Å.[69] Evidently, that there are a noticeable number of molecular pairs in cluster with intermolecular distances shorter than 25 Å. The dipolar interaction between them should induce spin−lattice relaxation, which broadens the TREPR spectrum of TEMPO in glassy environment.

(22) Alba, C.; Busse, L. E.; List, D. J.; Angell, C. A. *J. Chem. Phys.* **1990**, *92*, 617.

(23) Doss, A.; Hinze, G.; Schiener, B.; Hemberger, J.; Böhmer, R. *J. Chem. Phys. A* **1997**, *107*, 1740.

(24) Brickmann, J.; Kothe, G. *J. Chem. Phys.* **1973**, *59*, 2807.

(25) According to ref 24, the quartet spectrum represents a broad spectrum with a width of $4D_Q/g_e\beta_B$, with three peaks and the wings. The central peak is mainly due to the $-^1/_2 \leftrightarrow +^1/_2$ transition and includes contributions from the molecules of any orientations, while two outermost peaks, located at distance of $D_Q/g_e\beta_B$ from the central one, are mainly due to the $+^1/_2 \leftrightarrow +^3/_2$ and $-^3/_2 \leftrightarrow -^1/_2$ transitions and include predominantly the contributions from the molecules, which rotational axis is oriented perpendicular with respect to the magnetic field.

(26) Kallay, M.; Nemeth, K.; Surjan, P. R. *J. Phys. Chem. A* **1998**, *102*, 1261.

(27) Mizuochi, N.; Ohba, Y.; Yamauchi, S. *J. Chem. Phys.* **1999**, *111*, 3479.

(28) Samanta, A.; Kamat, P. V. *Chem. Phys. Lett.* **1992**, *199*, 635.

(29) Guijzemann, O. L. J.; Kaufman, F.; Porter, G. *J. Chem. Soc., Faraday Trans. 2* **1973**, *69*, 727.

(30) Yonemura, H.; Noda, M.; Hayashi, K.; Takudome, H.; Moribe, S.; Yamada, S. *Mol. Phys.* **2002**, *100*, 1395.

(31) Araki, Y.; Luo, H. X.; Islam, S. D. M.; Ito, O.; Matsushita, M. M.; Iyoda, T. *J. Phys. Chem. A* **2003**, *107*, 2815.

(32) Ishida, T.; Shinozuka, K.; Nogami, T.; Kubota, M.; Ohashi, M. *Tetrahedron* **1996**, *52*, 5103.

(33) Murov, S.; Carmichael, I.; Hug, G. *Handbook of Photochemistry*; Marcel Dekker Inc.: New York, 1993.

(34) Conti, F.; Corvaja, C.; Maggini, M.; Scorrano, G.; Ceroni, P.; Paolucci, F.; Roffia, S. *Phys. Chem. Chem. Phys.* **2001**, *3*, 3518.

(35) Allemand, P. M.; Koch, A.; Wudl, F.; Rubin, Y.; Diederich, F.; Alvarez, M. M.; Anz, S. J.; Whetten, R. L. *J. Am. Chem. Soc.* **1991**, *113*, 1050.

(36) ET between C_{60} and TEMPO may be partial, i.e., occurring via an exciplex ($C_{60}^{\delta\bullet-}\cdots TEMPO^{\delta+}$). Decay of this exciplex results in the ground state formation.[31.]

(37) Blank, A.; Levanon, H. *J. Phys. Chem.* **2001**, *105*, 4799.

(38) Imamura, T.; Onitsuka, O.; Obi, K. *J. Phys. Chem.* **1986**, *90*, 6741.

(39) Jenks, W. S.; Turro, N. J. *Res. Chem. Intemed.* **1990**, *13*, 237.

(40) Obi, K.; Imamura, T. *Rev. Chem. Intermed.* **1986**, *7*, 225.

(41) Saiful, I. S. M.; Fujisawa, J.; Kobayashi, N.; Ohba, Y.; Yamauchi, S. *Bull. Chem. Soc. Jpn.* **1999**, *72*, 661.

(42) Steiner, U. *Ber. Bunsen-Ges. Phys. Chem.* **1981**, *85*, 228.

(43) Savitsky, A. N.; Paul, H. *Chem. Phys. Lett.* **2000**, *319*, 403.

(44) Rozenshtein, V. B.; Gershenzon, Y.; Nalbandian, A. B. *Magnetic Resonance in Gases*; Academy of Sciences: Erevan, 1987.

(45) Guldi, D. M.; Prato, M. *Acc. Chem. Res.* **2000**, *33*, 695.

(46) Razi Neqwi, K. *J. Phys. Chem.* **1981**, *85*, 2303.

(47) Turro, N. J. *Modern Molecular Photochemistry*; Benjamin/Cummings Publishing Co., Inc.: Menlo Park, NJ, 1978.

(48) Medvedev, E. S.; Osherov, V. I. *Radiationless Transitions in Polyatomic Molecules*; Springer: Berlin, 1995.

(49) de Vault, D. *Q. Rev. Biophys.* **1980**, *13*, 384.

(50) Saik, V. O.; Goun, A. A.; Nanda, J.; Shirota, K.; Tavernier, H. L.; Fayer, M. D. *J. Phys. Chem. A* **2004**, *108*, 6696.

(51) Langen, R.; Chang, I. J.; Germanas, J. P.; Richards, J. H.; Winkler, J. R.; Gray, H. B. *Science* **1995**, *268*, 1733.

(52) Alexandrov, I. V. *Theory of Magnetic Relaxation*; Nauka: Moscow, 1975.

(53) Schwoerer, M.; Sixl, H. *Z. Naturforsch.* **1969**, *24a*, 952.

(54) Verma, N. C.; Fessenden, R. W. *J. Chem. Phys.* **1976**, *65* 2139.

(55) Poole, C. P. *Electron Spin Resonance: A Comprehensive Treatise on Experimental Techniques*, 2nd ed.; Dover Publications: London, 1997.

(56) For modeling a signal filter we have utilized in some simulations a specific filter function (a highpass Butterworth function with a cutoff frequency of 100 Hz). The result was close to that obtained by a simple subtraction of the equilibrium population difference.

(57) For **1** at $T \geq 300$ K, absorptive ESP lasts longer than theory predicts (cf. Figure 2 (part a1)). The presence of weakly interacting associated species can be invoked to explain long-lasting polarization in solution.

(58) To check the sensitivity of solving eqs 11 towards the initial conditions we have carried out computation when the lower sublevels of $^2T_1$ and $^4T_1$ were less populated than the upper ones. We discovered that the initial difference of 10^{-4} in the relative populations of the Zeeman sublevels almost does not affect the values of the simulation parameters (e.g., J_{DT}, k_{CT}, etc) obtained for the equally populated sublevels.

(59) Atkins, P. W.; Dobbs, A. J.; McLauchlan, K. A. *Chem. Phys. Lett.* **1974**, *29*, 616.

(60) Fujisawa, J.; Ohba, Y.; Yamauchi, S. *J. Phys. Chem. A* **1997**, *101*, 434.

(61) Goudsmit, G.-H.; Paul, H. *Chem. Phys. Lett.* **1993**, *208*, 73.

(62) Gonen, O.; Levanon, H. *J. Chem. Phys.* **1986**, *84*, 4132.

(63) In addition, failure or success to detect the outer lines could be also associated with a fact that $W_0 < W_1$, with larger degree of this inequality for **1.** Actually, Knapp et al.[70] investigated atomic phosphorus in its quartet ground state, encapsulated in C_{60}, and found that upon lowering the temperature the outer lines broaden beyond detection.

(64) Anderson, J. L.; An, Y.-Z.; Rubin, Y.; Foote, C. S. *J. Am. Chem. Soc.* **1994**, *116*, 9763.

(65) Mizuochi, N.; Ohba, Y.; Yamauchi, S. *J. Phys. Chem. A* **1999**, *103*, 7749.

(66) Kobori, Y.; Sekiguchi, S.; Akayama, K.; Tero-Kubota, S. *J. Chem. Phys. A* **1999**, *103*, 5416.

(67) Kobori, Y.; Yago, T.; Akiyama, K.; Tero-Kubota, S.; Sato, H.; Hirata, F.; Norris, J. R. *J. Phys. Chem. B* **2004**, *108*, 10226.

(68) Grest, G. S.; Cohen, M. H. *Adv. Chem. Phys.* **1981**, *48*, 455.

(69) Dzuba, S. A.; Kodera, Y.; Hara, H.; Kawamori, A. *Chem. Phys. Lett.* **1993**, *214*, 621.

(70) Knapp, C.; Weiden, N.; Kass, H.; Dinse, K.-P.; Pietzak, B.; Waiblinger, M.; Weidinger, A. *Mol. Phys.* **1998**, *95*, 999.